



Application of a Bio-waste Einkorn (*Triticum monococcum* L.) Husks Adsorbent for Removal of Metanil Yellow and Methylene Blue from Aqueous Media with Equilibrium, Kinetic, and Thermodynamic Studies

Baris Kocabiyik · Yuksel Bayrak

Received: 21 July 2023 / Accepted: 20 February 2024 / Published online: 7 March 2024
© The Author(s) 2024

Abstract In this study, the activated carbon (TmAC) with a high surface area and appropriate pore distribution was produced from einkorn (*Triticum monococcum* L.) husks by using $ZnCl_2$ with chemical activation method. The efficiency of the obtained activated carbon on the adsorption of anionic (metanil yellow) and cationic (methylene blue) dyestuffs from aqueous solutions was investigated in more detail. In addition, the surface characterization of activated carbon was performed using thermogravimetric analysis–differential thermal analysis (TGA-DTA), elemental analysis, scanning electron microscopy (SEM) images, Brunauer–Emmett–Teller (BET) specific surface areas, N_2 adsorption–desorption isotherms, pore volumes, pore size distributions, and Fourier-transform infrared spectroscopy-attenuated total reflection (FTIR-ATR) spectra. The highest surface area of activated carbon was measured as $1321 \text{ m}^2 \text{ g}^{-1}$ at the carbonization temperature of $500 \text{ }^\circ\text{C}$ by using impregnation ratio ($w/w=2.0$). Batch method was used in adsorption experiments. The parameters affecting the adsorption studies such

as adsorbent concentration, initial dye concentration, adsorption time, temperature, and pH were investigated. The adsorption mechanisms of metanil yellow (MY) and methylene blue (MB) on activated carbon were explained by using isotherms (Langmuir, Freundlich, Temkin, and Dubinin-Radushkevich), kinetic models (pseudo-first-order and pseudo-second-order), and the thermodynamic parameters (Gibbs free energy, enthalpy, and entropy).

Keywords Einkorn (*Triticum monococcum* L.) husk · Activated carbon · Adsorption · Metanil yellow · Methylene blue

1 Introduction

Paint, textile, food, cosmetics, and paper industries use dyes and pigments for coloring. Commercially, there are over 100,000 varieties of dyes, and the annual production of dye stuff exceeds 700,000 t. It is estimated that approximately 280,000 t of dyes is discharged into water bodies on a global scale every year (Abbas & Trari, 2015; Erdoğan and Oğuz Erdoğan 2016; Kishor et al., 2021). Discharging dye-containing wastewater into streams and lakes creates an environmental pollution that affects the photosynthesis activity in the aquatic ecosystem by reducing the efficiency of light use by plants. Polluted water sources, which pose a serious threat to sustainable and long-term development worldwide, and especially those

B. Kocabiyik
Vocational Higher School of Technical Sciences, Tekirdag
Namik Kemal University, 59030 Tekirdag, Turkey
e-mail: bkocabiyik@nku.edu.tr

Y. Bayrak (✉)
Department of Chemistry, Trakya University,
22030 Edirne, Turkey
e-mail: yukselbayrak@trakya.edu.tr

contaminated with the dyes of industrial wastes, are mutagenic and carcinogenic (Aguayo-Villarreal et al., 2013; Azam et al., 2022; Duman et al., 2016). There is no certain method used for dye removal from different types of wastewaters. The method to be employed varies according to the specific characteristics of the wastewater. Mortada et al. (2023) have presented activated carbon prepared from rice husk by chemical activation with ZnCl_2 . The main aim is to reduce chemical oxygen demand from wastewater. The maximum removal of chemical oxygen is 45.5 mg g^{-1} . In general, physical, chemical, and biological treatment techniques are used to purify wastewater from various impurities. These techniques include electrochemical degradation (Gui et al., 2019; Song et al., 2010), photocatalytic degradation (Lu et al., 2019; Reza et al., 2017), coagulation-flocculation (Ihaddaden et al., 2022), membrane process (Aluigi et al., 2014; Benosmane et al., 2022), and adsorption (Ma et al., 2015; Unugul & Nigiz, 2020). Among these techniques, adsorption was probably the most efficient method for wastewater treatment. Its advantages are easy process, affordability, facile regeneration, absence of sludge formation, and the non-production of hazardous final or intermediate products (Azari et al., 2020). Additionally, other treatment processes are high cost and frequently fall down to treat a wide variety of dyes in wastewater (Valix et al., 2004). Particularly, activated carbons (ACs) have an important place among widely employed industrial adsorbents for managing environmental pollution, owing to their substantial porous structure, high adsorption capacity, and expansive specific surface area (Ahmad et al., 2021).

Activating agents, in the chemical activation process, encompass a variety of chemical reagents. These agents play a crucial dual role as dehydrating agents and oxidizers, impacting the pyrolytic decomposition process. Various activating agents interact with cellulose, hemicellulose, lignin, or polysaccharides within the carbon precursor, initiating diverse activation mechanisms. These agents also have the ability to obstruct the formation of tar or ash, thereby enhancing the overall carbon yield (Gao et al., 2020; Yahya et al., 2015). Specifically, reactive agents facilitate the generation and expansion of cavities and reticulated or latticed structures. In this regard, commonly employed chemical agents include ZnCl_2 , H_3PO_4 , KOH , NaOH , H_2SO_4 , CaO , and HF (Sosa et al., 2023). The widespread preference of ZnCl_2 during

the production of the adsorbent is due to the ease of synthesis, big porous size, high chemical capacity, and large specific surface area (Kumar & Jena, 2017; Xia et al., 2020; Yagmur et al., 2020). Moreover, various biomaterials, such as barley straw (Pallarés et al., 2018), oak acorn (Nourmoradi et al., 2018), rubber seed shell (Azani et al., 2019), watermelon rind (Üner et al., 2019), orange peel (Wei et al., 2019), olive stones (Saleem et al., 2019), and sappan wood (Du et al., 2020), are widely used in activated carbon production. They have been preferred not only to reduce the cost of production but also have high carbon yield. Einkorn (*Triticum monococcum* L.) husks, which have similar properties (sustainable, low cost, abundant carbon content, and agricultural bio-waste) with these biomaterials, were selected as a suitable adsorbent for TmAC in this study.

Cereals and their derivatives as staple foods are among the most trusted nutrients by the world population. In addition, they include substantial proportions of antioxidants, vitamins, microelements, beneficial fibers, and mineral matters (Brandolini et al., 2008; Dimov et al., 2019; Keçeli, 2019). One of these cereals, einkorn (*T. monococcum* L.) was the first species of wheat grown in the Southeast of Turkey about 12,500–11,000 years ago. One of the most important parts of biodiversity and local ancestral seeds of einkorn has a limited and regional production (Hendek Ertop, 2019). Nonetheless, there is a growing interest in this crop attributed to its nutritious grain (Nakov et al., 2018), suitability for low-input agriculture, and its remarkable resistance to pests and diseases (Brandolini et al., 2018), making it advantageous for organic farming practices. Additionally, cultivated einkorn serves as a valuable gene pool for enhancing the traits of wheat (Zaharieva & Monneveux, 2014). Nowadays, some producers try to reach industrial manufacture to enlarge manufacture ability by protecting their traditional product standards and converting their production stages to an industrial scale (Hendek Ertop, 2019). Einkorn husks were used to obtain TmAC (*T. monococcum* activated carbon) adsorbent by using ZnCl_2 with chemical activation due to their cheap and abundant waste biomaterial.

In this study, TmAC obtained from einkorn husk was used to remove of anionic and cationic dyes. As far as we know, both these dyes were comparatively given firstly four different adsorption isotherms and kinetic and thermodynamic studies. The surface

properties of the produced TmAC were characterized by convenient techniques, such as TGA-DTA, BET, SEM-EDX, and FTIR-ATR. The efficiency of TmAC as an adsorbent for the removal of MB and MY dyes from aqueous solutions was assessed through the modifying various parameters, including contact time, initial concentrations, temperature, and pH, which are known to impact on the adsorption process. The adsorbent amount of TmAC was checked for MY and MB removal from the aqueous solution. In addition, the adsorption mechanism of TmAC was clarified by isotherms and kinetic and thermodynamic studies.

2 Experimental Section

2.1 Materials

MY (acid yellow 36, color index (CI)-13,065, chemical formula, $C_{18}H_{14}N_3NaO_3S$, and molar mass = $375.38 \text{ g mol}^{-1}$) and MB (basic blue 9, CI-52015, chemical formula, $C_{16}H_{18}ClN_3S$, and molar mass = $319.85 \text{ g mol}^{-1}$) were bought from Sigma-Aldrich and Merck, respectively, to be used as adsorbates in the current study. Zinc chloride ($ZnCl_2$) and hydrochloric acid (HCl) were used in different steps of experiments. All chemicals were used without further purification.

2.2 Instruments

Centrifuge device (Avvel C12, 6000 rpm), digital titrator (Titronic Universal), thermostat-controlled shaking water bath (WiseBath), deionized (DI) water equipment (GFL 2002), oven (Binder ED115), and UV-vis spectrophotometer (Mecasys Optizen POP Series) were used in different steps of experiments. Thermogravimetric analysis (TGA-DTA, Exstar 6300) was performed to follow up the weight losses of the einkorn (raw material). The morphology of the einkorn and TmAC were examined by SEM-EDX (ZEISS, EVO-LS10). The elemental analysis of einkorn and TmAC were evaluated by Leco TrueSpec Micro model. Spectroscopic analyses of einkorn and TmAC were performed using FTIR-ATR (PerkinElmer Frontier). Moreover, BET analysis (sample degas micromeritic Flow Prep 060 and Micromeritics TriStar II 3020) was used for measuring the

micropore areas, specific surface areas, pore sizes, and micropore volumes.

2.3 Preparation of $ZnCl_2$ -Treated Activated Carbon

Einkorn (*T. monococcum* L.) husks were supplied from the Central Anatolia region of Turkey to attain this study. The raw biomaterial was dried at room temperature after being washed with DI water, and stored in sealed colored glass bottles without grinding process. For the activation process, the dried einkorn (*T. monococcum* L.) husks (10 g) and $ZnCl_2$ solution were mixed in different impregnation ratio (w/w) from 0.5 to 3 (6 samples). These solutions were then poured into flasks and refluxed for about an hour until they reached boiling temperature to thoroughly treat the einkorn husks and the chemical agent. Then, solutions were transferred to Petri dishes and dried at $105 \text{ }^\circ\text{C}$ in an oven along a day. After drying, carbonization process was optimized with 4 different temperatures (400, 500, 600, and $700 \text{ }^\circ\text{C}$). The highest surface area was obtained at $500 \text{ }^\circ\text{C}$ for 1 h. Einkorn (*T. monococcum* L.) husk activated carbon (TmAC) was treated with 0.1 M HCl solution in order to neutralize after carbonization and washed with DI water. TmAC with neutral pH value was dehydrated at $105 \text{ }^\circ\text{C}$. In addition, the optimum $ZnCl_2$ concentration was determined at different concentration of $ZnCl_2$ solutions. The surface areas of TmAC were taken by BET measurements.

2.4 Characterizations of TmAC

Thermogravimetric analysis of einkorn (*T. monococcum* L.) husks was carried out at a temperature ranging from 20 to $950 \text{ }^\circ\text{C}$ with a gradual temperature increase of $10 \text{ }^\circ\text{C min}^{-1}$, while maintaining a nitrogen flow of 20 mL min^{-1} . Nitrogen (N_2) adsorption-desorption experiments were conducted using Micromeritics TriStar II 3020 at partial pressure between 0 and 1 bar and liquid nitrogen temperature ($-196.15 \text{ }^\circ\text{C}$). Before BET measurements, samples of TmAC were degassed for 30 min at $105 \text{ }^\circ\text{C}$ and shortly after under vacuum for 240 min at $350 \text{ }^\circ\text{C}$ to discharge evaporating contaminants (Üner et al., 2019).

The surface morphology, porosity of both the raw material, and TmAC materials were taken by SEM-EDX. The functional groups of materials were determined by FTIR-ATR. The zero point of charge

(pH_{ZPC}) was determined as follows: An amount of 0.1 g TmAC was put into a flask and added KNO₃ solution (0.1 M, 50 mL). The necessary amounts of HCl or NaOH solutions (0.1 M) were added to set the initial pH value from 2 to 12. The final pH was determined by constant shaking in 48 h (rate of agitation 150 rpm) (Milonjić et al., 1975).

2.5 Experiments of Adsorption

The adsorption experiments were conducted using the batch method. In this approach, dye solutions were prepared by diluting dye stock solutions with water to achieve the desired concentrations and were then placed in Erlenmeyer flasks. Subsequently, TmACs were introduced into the flasks, which were then positioned in a thermostat-controlled shaker and agitated at 150 r min⁻¹ until adsorption equilibrium was attained at the specified temperature. Following this, the samples underwent centrifugation for 20 min at 4000 r min⁻¹ to separate solid and liquid phases. The remaining amounts of dye not adsorbed in the solutions were determined using UV–visible spectrophotometry at 434 and 665-nm wavelengths for MY and MB dyes, respectively. Employing this methodology, adsorption experiments were conducted to investigate the impacts of TmAC concentration (0.1–0.7 g L⁻¹), initial dye concentration (17.5–105.0 mg L⁻¹), and temperature (25–45 °C). The adsorbed dye amount per unit mass of TmAC q_e (mg g⁻¹) was calculated using the following equation (Daoud et al., 2019):

$$q_e = \frac{(C_0 - C_e)}{W} x V \quad (1)$$

and the percentage of dyes removal equation was calculated as follows:

$$Removal(\%) = \frac{(C_i - C_e)}{W} \times 100 \quad (2)$$

where C_i (mg L⁻¹) and C_e (mg L⁻¹) are the dye concentrations at initial and equilibrium, respectively. V is the volume of dye solution in liters, and W is the mass of TmAC adsorbent in grams.

The kinetic investigation primarily focuses on elucidating the mechanism of the adsorption process, wherein a system transitions from an initial state to a final state over time. To comprehend the kinetics, pseudo-first-order (PFO) and pseudo-second-order

(PSO) models were employed for testing. Both PFO and PSO kinetic models were developed and expressed in Eqs. 3 and 4, respectively (Lagergren, 1898; Zhang et al., 2015).

$$\log(q_e - q_t) = \log(q_e) - \frac{k_1}{2,303} \cdot t \quad (3)$$

where k_1 (min⁻¹) was the adsorption rate constant of PFO and q_e and q_t (mg g⁻¹) were adsorbed quantity of MY and MB dyes at equilibrium and at time t , respectively.

$$\frac{t}{q_t} = \frac{1}{k_2 q_e^2} + \frac{1}{q_e} t \quad (4)$$

where k_2 (g mg⁻¹ min⁻¹) was adsorption rate constant of PSO and q_e and q_t (mg g⁻¹) were adsorbed quantity of MY and MB dyes at equilibrium and at time t , respectively.

In this study, 4 different isotherm models, such as Langmuir (Langmuir, 1916), Freundlich (Freundlich, 1906), Temkin (Temkin & Pyzhev, 1940), and Dubinin-Radushkevich (D-R) (Dubinin & Radushkevich, 1947), were assessed at various temperatures for MY and MB dye adsorption.

For Langmuir isotherm model in Eq. 5, adsorption was linearly increased with the initial amount of adsorbate due to the uniformity of adsorption energy. Adsorbate concentration was directly proportional to the adsorption rate.

$$\frac{C_e}{q_e} = \frac{1}{q_{max} K_L} + \frac{C_e}{q_{max}} \quad (5)$$

where the capacity adsorption of monolayer at maximum was q_{max} (mg g⁻¹) and the adsorption constant of Langmuir model was K_L (L mg⁻¹).

The separation factor R_L (Parab et al., 2009; Weber & Chakravorti, 1974), equilibrium parameter or a dimensionless constant was derived from Langmuir expression, could be utilized to define the feasibility of the adsorption processing in Eq. 6:

$$R_L = \frac{1}{1 + K_L C_0} \quad (6)$$

R_L explained the absorption-processing nature and indicated if the adsorption processing was ($0 < R_L < 1$) positive, ($R_L = 1$) linear, ($R_L > 1$) negative, or ($R_L = 0$) non-reversible.

Freundlich isotherm model was defined as multi-layered adsorption (Eq. 7) (Hameed et al., 2008). The surface of multilayer was accepted as heterogeneous in terms of adsorption sites and energy.

$$\ln q_e = \ln K_F + \frac{1}{n} \ln C_e \quad (7)$$

where n (dimensionless) and K_F (mg g^{-1}) ($\text{L mg}^{-1/n}$) were constants depending on temperature, adsorbate, and adsorbent in Freundlich Eq. $1/n$ was the heterogeneous factor in the range of 0–1. The more heterogeneous surface was obtained if $1/n$ value was closer to zero. Adsorption; if ($0 < 1/n < 1$), it was considered desirable, ($1 < 1/n$) undesirable, and ($1/n = 1$) irreversible (Ayawei et al., 2017).

Temkin isotherm model was based on the interaction between adsorbent and adsorbate, which assumed that the heat of adsorption decreased linearly with increasing degree of adsorption process (Ganguly et al., 2020; Wang et al., 2018) in Eq. 8:

$$q_e = \frac{RT}{B_T} \ln(A_T C_e) \quad (8)$$

where B_T was symbolized Temkin isotherm constant (J mol^{-1}), A_T was given as Temkin isotherm equilibrium binding constant (L g^{-1}), R was defined as universal gas constant ($8.314 \text{ J mol}^{-1} \text{ K}^{-1}$), and T was represented as absolute temperature of solution in K.

D-R isotherm model was generally used to express the adsorption mechanism with the distribution of Gaussian energy on heterogeneous surfaces. The characteristic sorption curve was related to the porous structure of the sorbent (Alberti et al., 2012; Celebi et al., 2007).

$$\ln q_e = \ln q_d - \beta \varepsilon^2 \quad (9)$$

$$\varepsilon = RT \ln \left[1 + \frac{1}{C_e} \right] \quad (10)$$

$$E = \frac{1}{\sqrt{2\beta}} \quad (11)$$

where q_d was symbolized D-R constant (mg g^{-1}), β was given constant related to free energy, ε was Polanyi potential, and E was mean free energy (kJ mol^{-1}). The physical and chemical adsorption process was applied using Eq. 11. If $E < 8 \text{ kJ mol}^{-1}$, it

was determined as physical adsorption. However, if $8 < E < 16 \text{ kJ mol}^{-1}$, it was dominated as chemical adsorption (Chowdhury & Saha, 2010; Olasehinde et al., 2020).

The spontaneous, randomness, and endothermic or exothermic behavior of adsorption process were obtained by thermodynamic parameters, such as Gibbs free energy (ΔG°), entropy (ΔS°), and enthalpy (ΔH°), respectively. These parameters were calculated by applying the experimental values obtained from MY and MB adsorption on TmAC in the following equations (Hassan et al., 2020; Rahman et al., 2017).

$$\Delta G^\circ = -RT \ln K_C \quad (12)$$

$$\Delta G^\circ = \Delta H^\circ - T \Delta S^\circ \quad (13)$$

$$\ln K_C = \frac{\Delta S^\circ}{R} - \frac{\Delta H^\circ}{R} \frac{1}{T} \quad (14)$$

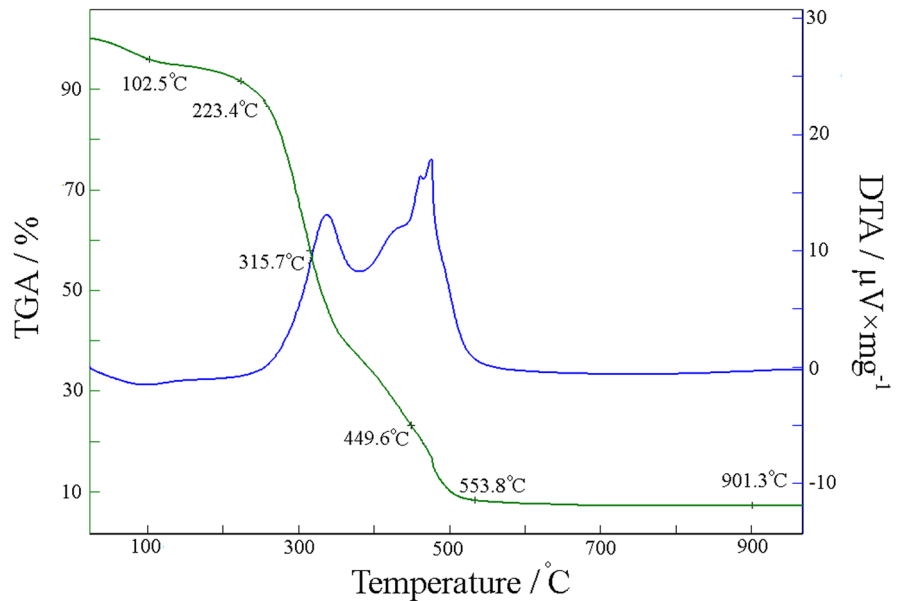
where R was gas constant ($8.314 \text{ J mol}^{-1} \text{ K}^{-1}$), T was absolute temperature in Kelvin T , and K_C was equilibrium constant, which was obtained from Langmuir constant.

3 Results and Discussion

3.1 TGA-DTA Analysis of Einkorn

The thermal behaviors of the materials during the carbonization and activation process were investigated by TGA-DTA. The thermograms of einkorn (*T. monococcum* L.) husks are depicted in Fig. 1. The first mass loss was seen in the degradation of material in Fig. 1 from 102.5 to 223.4 °C.

This first stage corresponds to the drying period in einkorn husks during the volatile solvents, especially water molecules. The first degradation was completed with small weight loss (less than 10%) as found by Zhang et al. (2017). Devolatilization is the most important step in all thermochemical conversion processes involving biomass. This step is the second decomposition step, corresponding to a significant reduction in the mass of the sample (~80%). In this step, volatile hydrocarbon was set free due to the fast thermal decomposition of hemicelluloses, cellulose, and some of the lignin. It occurs at a temperature between 200 °C and 500 °C, where

Fig. 1 TGA-DTA of 50 mesh and smaller einkorn

the remarkable slope of the thermal analysis curves is observed (Abdullah et al., 2010). In the last stage, there was no significant loss of mass after 500 °C, the inorganic materials do not melt, and the degradation continues at very low rates till its end. For this reason, the carbonization process for the production of TmAC from the starting material was carried out at temperatures between 400 and 700 °C (Nirmaladevi & Palanisamy, 2019). In a study conducted by Avelar et al. (2010) on the utilization of piassava fibers in the preparation of activated carbon, it was reported that the differential thermal analysis curve exhibited a broad band around 320 °C, attributed to the decomposition of hemicellulose, cellulose, and lignin, with a maximum point at approximately 378 °C. Similarly, einkorn is shown in Fig. 1 with a shoulder at about 340 °C and a maximum peak at 490 °C and also shows a broad band in DTA. It also shows an exothermic behaviour of the einkorn.

3.2 Elemental Analysis of Einkorn and TmAC

The elemental analysis of einkorn and TmAC is listed Table 1. The weight percent of C element in TmAC was remarkably raised from 40.58 to 77.33% after activation process of einkorn. However, the weight percent of oxygen element was sharply decreased from 50.87 to 15.94%. In addition, the weight percents of hydrogen and nitrogen elements

Table 1 The elemental analysis of einkorn and TmAC with impregnating ratio 1/2 (w/w)

Elements	Einkorn (wt%)	TmAC (wt%)
Carbon	40.58	77.33
Hydrogen	5.50	3.81
Nitrogen	0.95	0.77
Sulfur	2.10	2.15
Oxygen (by difference)	50.87	15.94

were gradually lower in TmAC. On the contrary, the weight percent of sulfur element seems to be comparable between einkorn and TmAC. During chemical activation and carbonization process of einkorn husk, oxygen, nitrogen, and hydrogen gases easily leave from einkorn husk due to the volatile gases. Probably, this process produced a rich carbon product of lower functional groups (low oxygen content).

3.3 BET Analysis of TmAC

The BET analysis of TmAC could be presented in the following parameters: surface area ($\text{m}^2 \text{g}^{-1}$), micropore area ($\text{m}^2 \text{g}^{-1}$), micropore volume ($\text{cm}^3 \text{g}^{-1}$), total pore volume ($\text{cm}^3 \text{g}^{-1}$), and average pore diameter (nm) (Table 2). Starting from an impregnation ratio of 0.5, the BET surface area progressively

Table 2 BET analysis of TmAC

ZnCl ₂ /einkorn (w/w) impregnation ratio	0.5	1.0	1.5	2.0	2.5	3.0
BET surface area (m ² g ⁻¹)	854.05	1164.52	1291.06	1321.01	1288.12	1224.61
Micropore area (m ² g ⁻¹)	567.12	312.16	163.47	106.42	89.90	109.43
Micropore volume (cm ³ g ⁻¹)	0.26	0.13	0.06	0.03	0.03	0.04
Total pore volume (cm ³ g ⁻¹)	0.45	0.71	0.97	1.22	1.34	1.52
Average pore diameter (nm)	2.08	2.44	3.00	3.68	4.16	4.97

risers, reaching its peak at an impregnation ratio of 2.0 (1321.01 m² g⁻¹). However, a further increase in the impregnation ratio to 3.0 results in a slight decrease in the BET surface area to 1224.61 m² g⁻¹. The data indicates that there is an optimal impregnation ratio (around 2.0) that maximizes the BET surface area of the activated carbon. As a result, the optimum ZnCl₂/einkorn (w/w) impregnation ratio was assessed as 2.0 for the activation treatment.

The physisorption isotherms, approximately in the last 30 years, have been updated from the classification proposed by IUPAC into six types, associated with specific pore structures, since their initial categorization (Sing et al., 1985), to their current state (Thommes et al., 2015). Many variants of hysteresis loops have been reported in six characteristic types (Thommes et al., 2015). When the N₂ adsorption–desorption isotherm was examined, it resembles the reversible type I isotherm, resulting to micropore structures at impregnation ratio of 0.5. However, when impregnation ratio was risen to 2.0, the mesoporous structures were obtained from the hysteresis loops and look like type IV isotherms. As a result, ZnCl₂/einkorn (w/w) impregnation ratio was obtained as 2.0 (optimum value); the hysteresis loops and pore shape were obtained as type H4 and a narrow capillary cleft, respectively Fig. 2.

3.4 SEM–EDX Analysis of Einkorn and TmAC

The high-resolution SEM images of einkorn and TmAC are shown in Fig. 3. There was a surface morphology difference between einkorn (Fig. 3a, b) and TmAC (Fig. 3c, d). Both images of einkorn (a and b) have no porosity, and flat capillary surfaces. However, the surfaces of TmAC (c and d) have irregular caves and pores with a heterogeneous structure after the activation process, and these findings were also noticed by Chen et al. (2011). Both BET analysis

and SEM images of TmAC obtained from einkorn with chemical activation (ZnCl₂) are suitable for the adsorption experiments.

The EDX analysis of einkorn and TmAC is shown in Table 3. The results of EDX analysis were similar to elemental analysis results (Table 1). The weight percent of carbon element in the total content increased from 49.11 to 83.25%, but the weight percent of oxygen element in total content decreased from 47.70 to 10.52% after the activation process. In addition, due to the treatment of ZnCl₂ as an activation agent, there was an increase of weight percent of zinc and chloride elements in total content of TmAC.

3.5 FTIR-ATR Analysis of Einkorn and TmAC

The FTIR-ATR analysis of einkorn and TmAC was obtained to understand the structure of the functional groups (Fig. 4). The broad and strong peak of einkorn was referred at 3295 cm⁻¹ by overlapping of O–H and N–H stretching in lignin, pectin, cellulose, and hemi-cellulose (He et al., 2021). The peak at 2912 cm⁻¹ was attributed by the symmetric and asymmetric stretching in CH₃ and aliphatic CH₂ (Kang et al., 2019). The weak band positioned at 1632 cm⁻¹ was conformed to stretching vibration of C=C bonds in aromatic groups of lignin or benzene rings (Prakash et al., 2021). The strong peak at 1032 cm⁻¹ was pertaining to O–H bending and C–O stretching vibrations in alcohols and carboxylic acids (Dağdelen et al., 2014; Hesas et al., 2013). When the FTIR spectra of einkorn and TmAC were compared with each other, it was clearly seen that the peaks of TmAC exhibited less adsorption bands (less transmittance %). This suggests that various functional groups present in the raw material spectrum disappear after the carbonization and activation steps. Additionally, it can be attributed to the molecular convergence within the TmAC caused

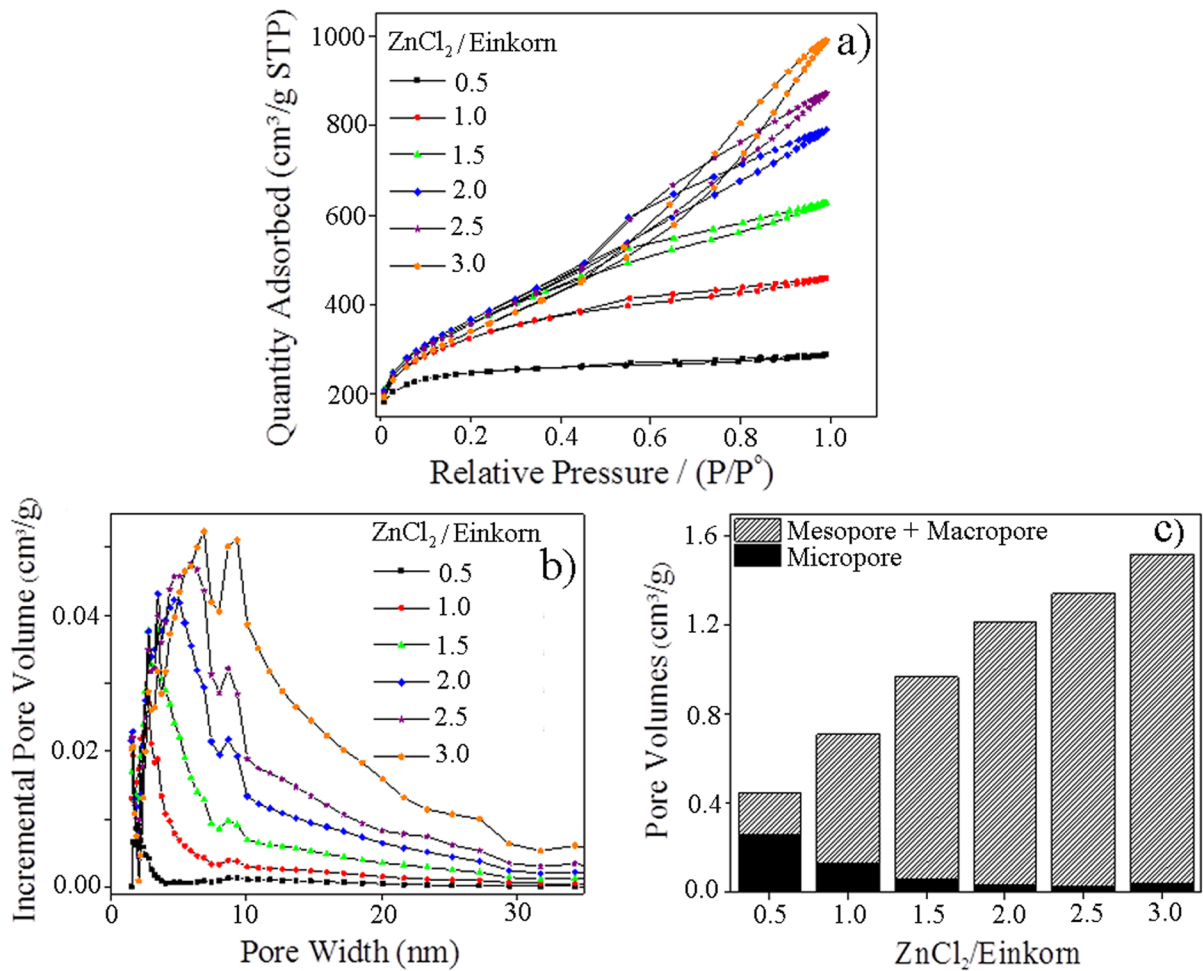


Fig. 2 a N_2 adsorption–desorption isotherms, b pore size distributions, and c pore volumes at 77 K of TmAC

by the high carbonization temperature (500 °C). This convergence continues without degradation throughout subsequent cooling, neutralization, and washing processes.

3.6 pH_{PZC} of TmAC

The point of zero charge of pH (pH_{PZC}) value of the adsorbent was given as a fundamental feature of interphase properties. The surface chemistry of any material like carbon can be predicted by the acidic or basic nature of its surface. Density of positive charges (cations) equals that of negative charges (anions) was

accepted as pH_{PZC} . pH_{PZC} of TmAC was obtained as 7.33 shown in Fig. 5.

3.7 Effect of Adsorbent Concentration for MY and MB

The effect of adsorbent concentration on the percentage of dye removal was carried out in the following parameters: agitation rate of 150 rpm, temperature of 25 °C, and dye initial pH value are shown in Fig. 6a, b for MY and MB, respectively. The percentage of MY dye removal significantly increased from 68.27 to 98.73% when the activated carbon concentration increased from 0.1 to 0.3 g

Fig. 3 SEM images of einkorn: **a** 100 \times , **b** 500 \times and TmAC, **c** 100 \times , and **d** 500 \times

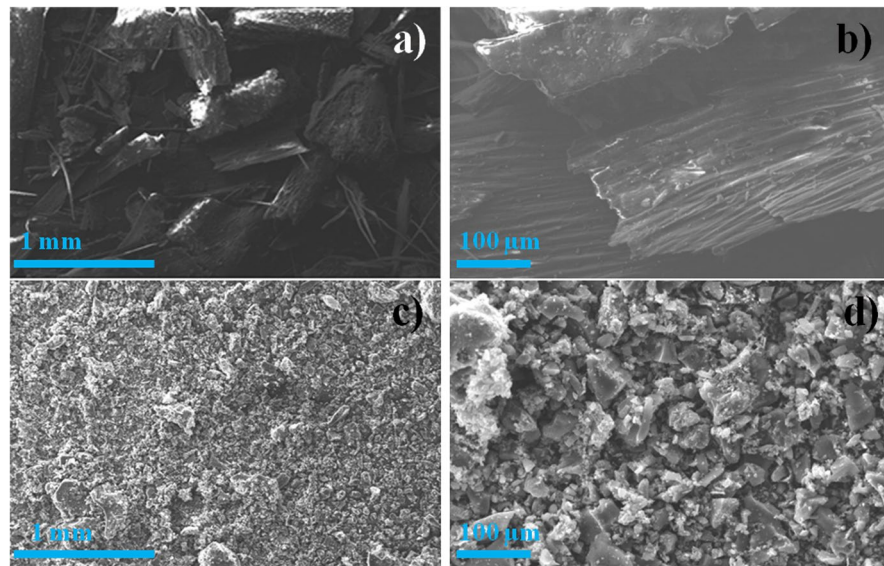


Table 3 EDX spectra with element contents of the einkorn and TmAC

Elements	Einkorn (wt%)	TmAC (wt%)
C	49.11	83.21
O	47.70	10.52
Si	1.51	1.36
K	0.88	0.00
Ca	0.38	0.00
Cl	0.13	2.41
Mg	0.12	0.67
S	0.09	0.23
Al	0.08	0.00
Zn	0.00	1.61
Total	100.00	100.00

L^{-1} (Fig. 6a). Further increases in activated carbon concentration, i.e., from 0.4 to 0.7 $g L^{-1}$, the percentage of dye removal was almost unchangeable. Therefore, the adsorbent concentration was determined as 0.3 $g L^{-1}$ for MY, and this amount was used in the adsorption experiments. Similarly, adsorbent concentration of MB was obtained from different TmAC concentrations from 0.1 to 0.5 $g L^{-1}$ (Fig. 6b). The percentage removal of MB raised from 54.34 to 99.29%. Thereafter, there was no significant increase of percentage of dye removal of

MB from 0.55 to 0.7 $g L^{-1}$ (Fig. 6b). The optimum concentration of TmAC was chosen as 0.5 $g L^{-1}$ due to the stable concentration of MB. The adsorbent concentration difference was obtained by chemical structures of MY and MB dyes.

3.8 The Effects of Contact Time and Initial Dye Concentration for MY and MB

The effects of contact time versus dye removal of MY and MB (%) are given at different dye concentrations in Fig. 7a, c, respectively. In addition, the effects of initial dye concentration of MY and MB versus percentages of dye removal (%) are shown in Fig. 7b, d, respectively. For both MY and MB dyes, the figures reveal that an increase in contact time positively influences TmAC dye removal, while an increase in the initial dye concentration has a negative impact. Although the percentage of dye removal of MY and MB at 17.5 $mg L^{-1}$ was obtained as 99.03% and 99.57%, respectively, the percentage of dye removal of MY and MB at 105.0 $mg L^{-1}$ was obtained as 77.45% and 74.01%, respectively. Furthermore, the duration required to reach equilibrium extended with the rise in dye concentration. As an illustration, for the initial dye concentration of 17.5 $mg L^{-1}$, equilibrium was reached in 45 and 40 min, while for the initial dye concentration of 105.0 $mg L^{-1}$, equilibrium

Fig. 4 FTIR-ATR spectra of einkorn and TmAC

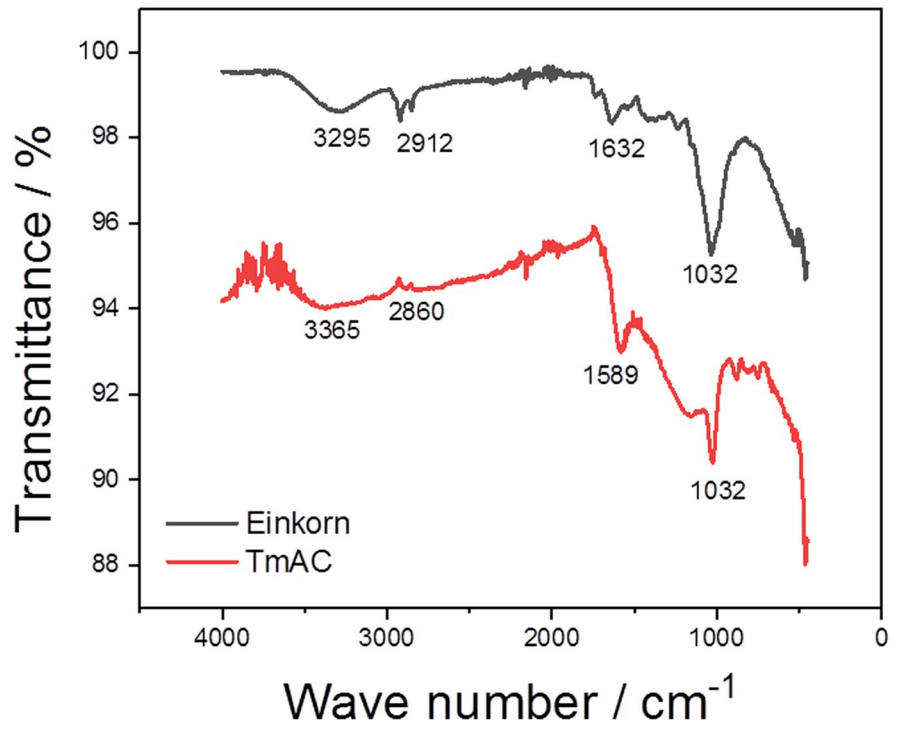
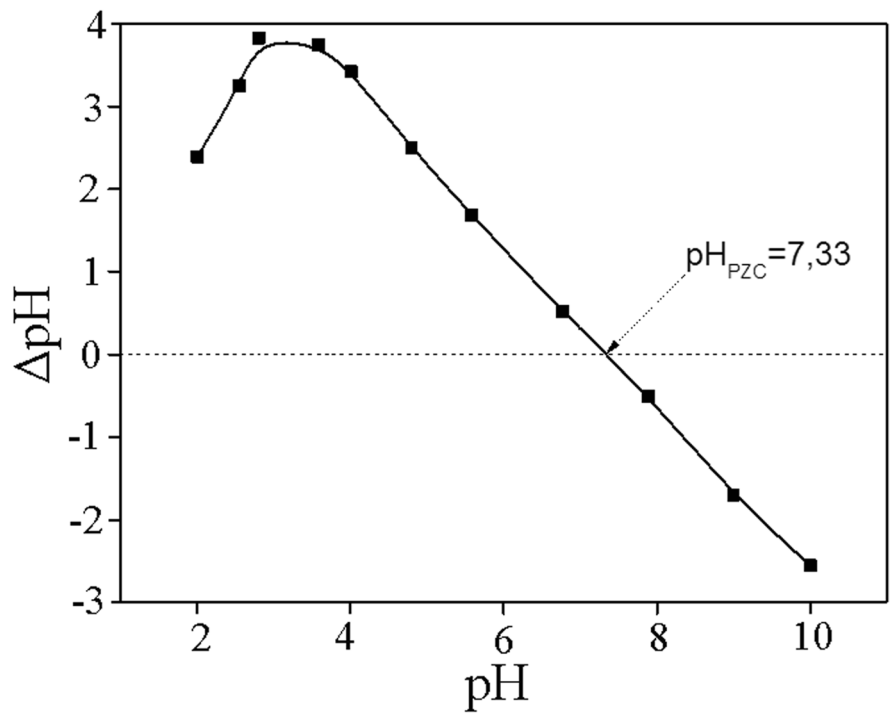


Fig. 5 pH_{PZC} of TmAC



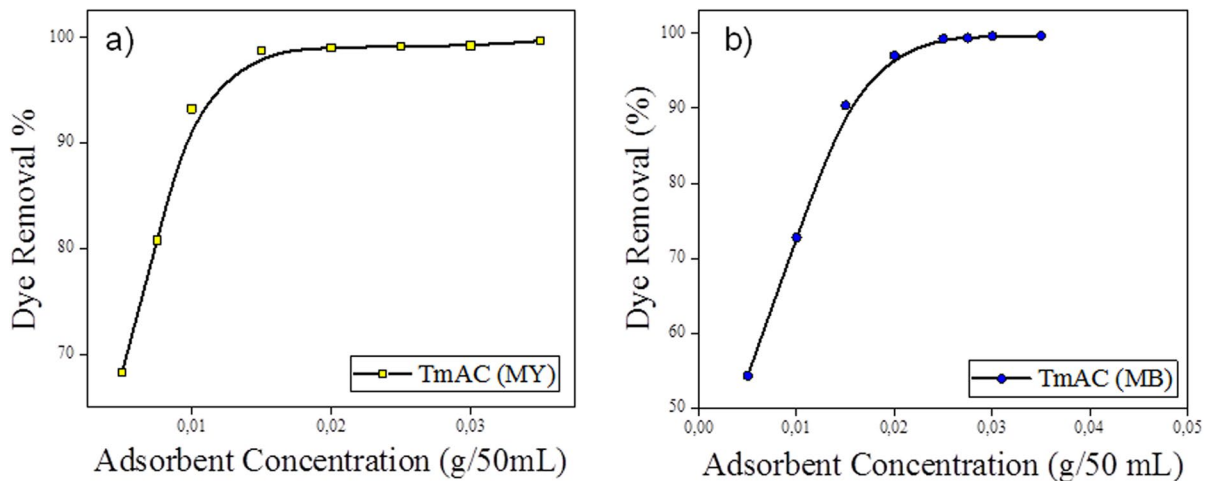


Fig. 6 Adsorbent concentration effect on dye removal: **a** MY and **b** MB. (Temperature 25 °C, rate of agitation 150 rpm, pH initial pH)

was achieved after 270 and 200 min for MY and MB, respectively. Therefore, the increase in the electrostatic repulsion forces between the dye molecules in solution and the dye molecules adsorbed by TmAC occurred with the increase in the initial dye concentration (Geçgel et al., 2016).

Based on observations from SEM and BET analysis results, it can be inferred that the surface of TmAC is likely to have a porous structure. Due to the hollow nature of the pores within this porous structure, the removal of MY and MB dyes occurred rapidly at the beginning of the contact time. After a certain period, as the empty pores filled with dye molecules, the reduction in binding rate led to the establishment of adsorption equilibria (Geçgel et al., 2015).

3.9 Effect of Temperature on MY and MB Adsorption

The effect of temperature on MY and MB removal from aqueous solution was studied for six different dye concentrations from 17.5 to 105.0 mg L⁻¹ at four different temperatures from 15 to 45 °C, respectively (Fig. 8a, b). By increasing of temperature from 15 to 45 °C, the percentage removal of MY and MB was slightly raised from 98.43 to 99.76% and from 99.53 to 99.70% at 17.5 mg L⁻¹, respectively. Similarly, the temperature increased from 15 to 45 °C, and the percentage removal of MY and MB rose from 73.03 to

74.27% and from 69.88 and 74.01% at 105.0 mg L⁻¹, respectively. As a result, both MY and MB at the initial concentration from 17.5 to 105.0 mg L⁻¹, temperature versus the percentage removal of dye concentrations were gone up together between the temperature of 15 to 45 °C. Thus, the heat behavior of MY and MB adsorption on TmAC was resulted in endothermic behavior.

3.10 Effect of pH on MY and MB Adsorption

pH is an important parameter on the adsorption of MY and MB (Benhachem et al., 2019). When the pH value was raised from 2 to 11, the percentage removal of MY was decreased from 98.03 to 75.11% (Fig. 9a). Surface charge information was obtained from pHPZC. It was set as 7.33 for TmAC as found above. For pH values below 7.33, TmAC surface was positively charged. On the contrary, for pH values above 7.33, TmAC surface was negatively charged. The percentage removal of MY increased at pH value below 7.33 due to the electrostatic attraction of the positively charged TmAC (pH dependent charge) and MY dye molecules (anionic form) in spite of the fact that the percentage removal of MY was decreased at pH value above 7.33 due to the electrostatic repulsive of TmAC and MY dye molecules.

Unlike adsorption of MY, the percentage removal of MB was decreased at pH value below 7.33 due to the electrostatic repulsive of TmAC and MB dye

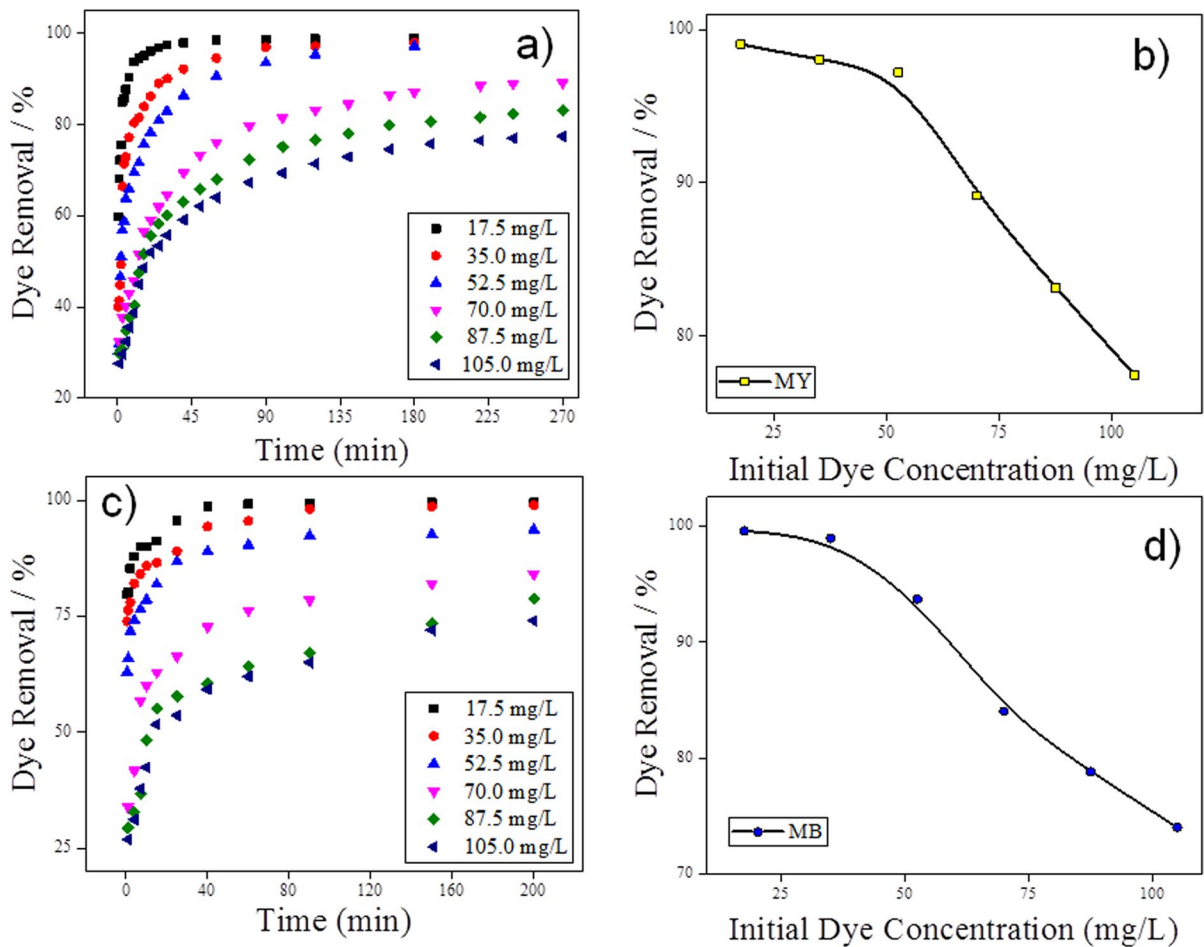


Fig. 7 Effects of contact time versus dye removal (%) of **a** MY and **c** MB. Effects of initial dye concentrations of versus percentages of dye removal (%) of **b** MY and **d** MB. Temperature

25 °C, rate of agitation 150 rpm, pH: initial pH, concentration of adsorbent for MY and MB were taken in 0.015 g/50 mL and 0.025 g/50 mL, respectively

molecules (cationic from) in spite of the fact that the percentage removal of MB was increased at pH value above 7.33 due to the electrostatic pulls of TmAC and MB dye molecules.

3.11 Kinetic Studies

The adsorption time and mechanism were explained using kinetic models. Time-dependent kinetic models were applied in liquid adsorption studies, called as pseudo-first-order (PFO) and pseudo-second-order (PSO) kinetic models. Batch adsorption kinetic studies of MY and MB dye molecules were performed to

investigate the effective adsorbate-adsorbent contact time and step of the adsorption reaction rate (Özacar et al., 2008).

The q_e and k_1 parameters of MY and MB dye molecules could be determined in different initial concentrations (C_0) at 25 °C by the intercepts and slopes of the lines according to the plots of $\log(q_e - q_t)$ vs. t , respectively (Fig. 10a, b). Likewise, the q_e and k_2 parameters of MY and MB dye molecules were calculated according to the plots of t/q_t vs. t , respectively (Fig. 10c, d). Kinetic parameter constants were given for different initial concentrations of MY and MB dye

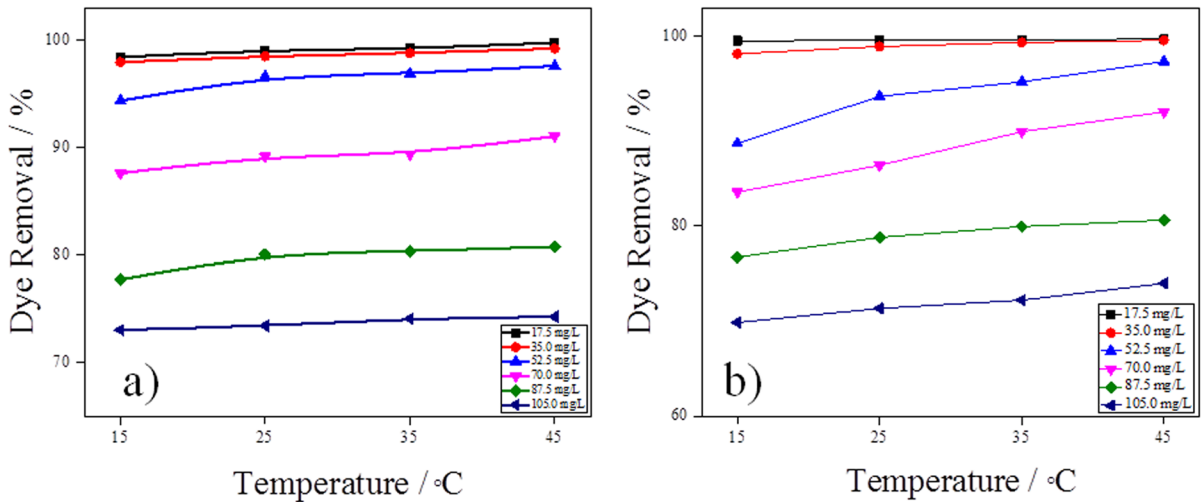


Fig. 8 Effects of temperature versus dye removal (%) of **a** MY and **b** MB. Rate of agitation 150 rpm, pH: initial pH, concentration of adsorbent for MY and MB were taken in 0.015 g/50 mL and 0.025 g/50 mL, respectively

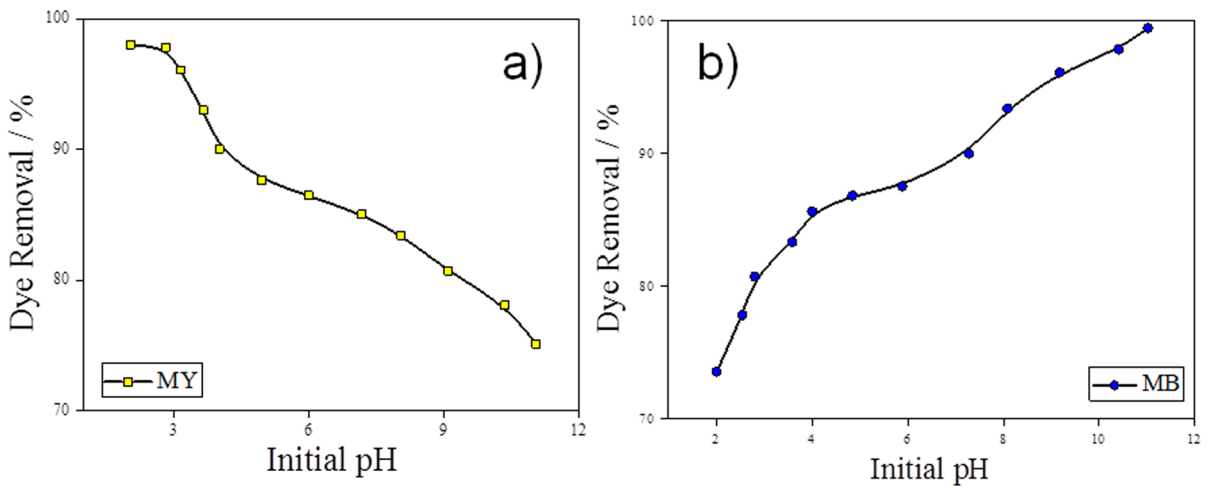


Fig. 9 Effects of initial pH versus dye removal (%) of **a** MY and **b** MB. Agitation speed 150 rpm, temperature 25 °C, contact time 90 min, dye concentration 35.0 mg L⁻¹, concentration

of adsorbent for MY and MB were taken in 0.015 g/50 mL and 0.025 g/50 mL, respectively

molecules in Table 4. PSO plots of MY and MB dye molecules fitted the $q_{e(exp)}$ and $q_{e(cal)}$ better than PFO as shown in Fig. 10c, d. The adsorption rate fitted PSO kinetic model for both MY and MB dye adsorptions. Kinetic parameters were appropriate for $q_{e(exp)}$ and $q_{e(cal)}$. The values of correlation coefficients (R^2) with the kinetic

parameters in Table 4 supported that both MY and MB dye molecules on TmAC fit PSO kinetic model. It is because the correlation coefficients of PSO model ($R^2 > 0.994$) were quite higher than correlation coefficients of PFO model ($R^2 < 0.987$) for all initial MY and MB concentrations at 25 °C.

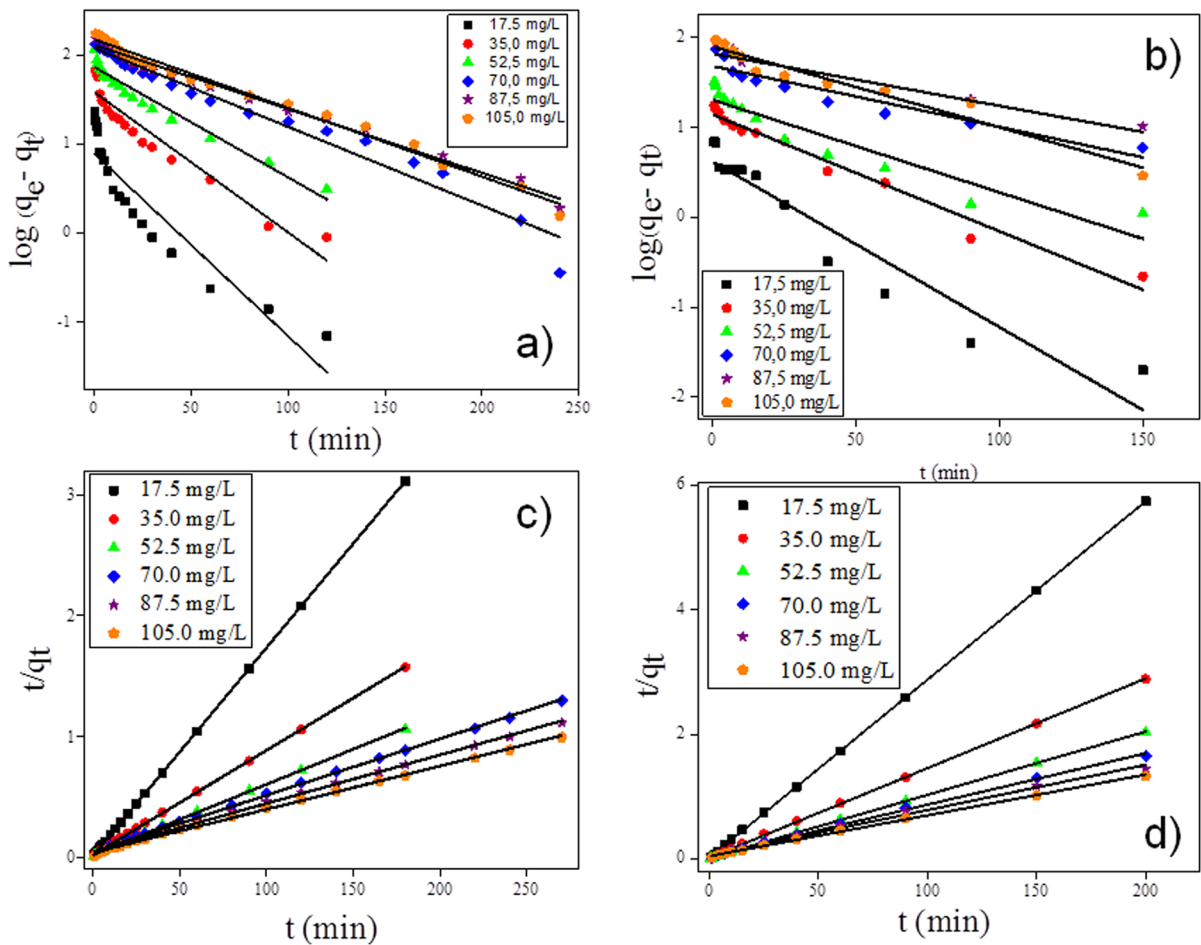


Fig. 10 PFO model: **a** MY and **b** MB and PSO model: **c** MY and **d** MB

3.12 Equilibrium Studies

The principal information was supplied by adsorption equilibrium isotherms from adsorbate particles, which were dispersed among liquid or solid phases to evaluate the capability and compatibility of an adsorbent. The better suitability of adsorption of isotherm was found by applying the experimental data to all isotherm equations. Isotherm type was determined drawing a linear plot as shown in Figs. 11 and 12. Adsorption isotherm parameters of Langmuir, Freundlich, Dubinin Raduskevich, and Temkin isotherm models are presented in Table 5 for MY and MB dyes on TmAC at 25 °C. Langmuir isotherm model was determined as the best-fitted adsorption model for both the system of MY/TmAC and MB/TmAC. The maximum adsorption

capacities for MY/TmAC and MB/TmAC were calculated as 266.67 mg g⁻¹ and 151.52 mg g⁻¹, respectively.

Adsorption capacity (q_{\max}) is an important parameter for comparison of other adsorbents. Max. adsorption capacities (q_{\max}) of other studies are given from literatures in Table 6.

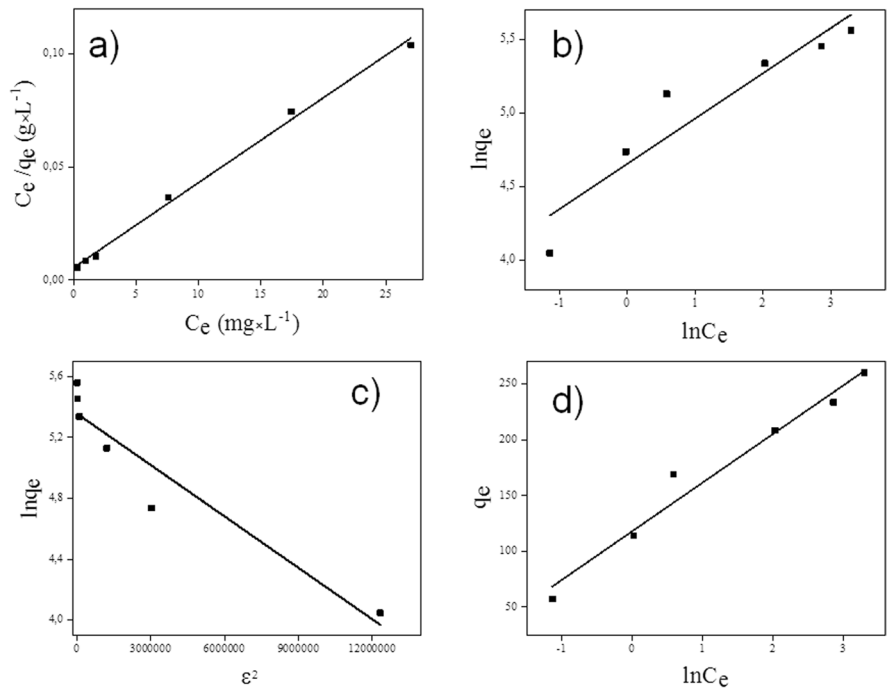
3.13 Thermodynamic Studies

ΔH° And ΔS° values were derived from the slope and intercept of the Van't Hoff plot of $\ln K_C$ vs. $1/T$, respectively (Fig. 13a, b). Furthermore, ΔH° , ΔS° , and ΔG° values at various temperatures (298, 308, and 318 K) are listed in Table 7. The negative values of ΔG° showed spontaneous and feasible MY and MB adsorption on TmAC. According to

Table 4 Kinetic parameter constants for different initial concentrations of MY and MB

C_0 (mg L ⁻¹)	$q_{e, \text{exp}}$ (mg g ⁻¹)	Pseudo-first order (PFO)			Pseudo-second order (PSO)		
		q_e (mg g ⁻¹)	k_1 (min ⁻¹)	R^2	$q_{e, \text{cal}}$ (mg g ⁻¹)	$k_2 \times 10^{-3}$ (g mg ⁻¹ min ⁻¹)	R^2
MY							
17.5	57.14	7.880	0.0472	0.85108	57.971	29.52	1.00000
35.0	113.95	38.675	0.0363	0.91181	115.340	4.09	0.99981
52.5	169.03	73.877	0.0286	0.93993	171.527	1.67	0.99900
70.0	208.07	120.526	0.0204	0.96456	214.133	0.48	0.99873
87.5	233.57	130.828	0.0166	0.98608	248.756	0.38	0.99842
105.0	259.93	150.872	0.0178	0.98674	278.552	0.34	0.99837
MB							
17.5	34.84	4.144	0.0424	0.90563	34.953	45.91	0.99996
35.0	69.24	13.820	0.0299	0.97172	69.541	10.62	0.99980
52.5	98.36	20.155	0.0237	0.87617	98.522	7.10	0.99984
70.0	120.98	47.845	0.0156	0.88247	121.212	1.48	0.99781
87.5	137.92	65.993	0.0134	0.89035	137.931	0.84	0.99401
105.0	149.86	78.583	0.0206	0.94203	153.139	0.93	0.99807

Fig. 11 a Langmuir, b Freundlich, c D-R, and d Temkin isotherms of MY adsorption on TmAC. (Conditions: $V_{\text{MY}} = 50$ mL, adsorbent amount = 0.015 g, agitation rate = 150 rpm, adsorption temperature = 25 °C, and contact time = 270 min).



Eq. 13, the more efficient adsorption process was acquired at high temperatures ($\Delta G^\circ < 0$). If ΔH° value was less than 10 kcal mol⁻¹, the adsorption of MY and MB on TmAC was obtained as physical and reversible process. In addition, the positive value of ΔH° was indicated as endothermic

adsorption behavior. The randomness of MY and MB adsorption was defined as positive ΔS° value during penetration of dye molecules in pores of TmAC. As a result, the adsorption activity of both dye molecules increased the randomness (Auta & Hameed, 2011).

Fig. 12 **a** Langmuir, **b** Freundlich, **c** D-R, and **d** Temkin isotherms of MB adsorption on TmAC. Conditions: $V_{MB} = 50$ mL, adsorbent amount = 0.025 g, agitation rate = 150 rpm, adsorption temperature = 25 °C, and contact time = 200 min).

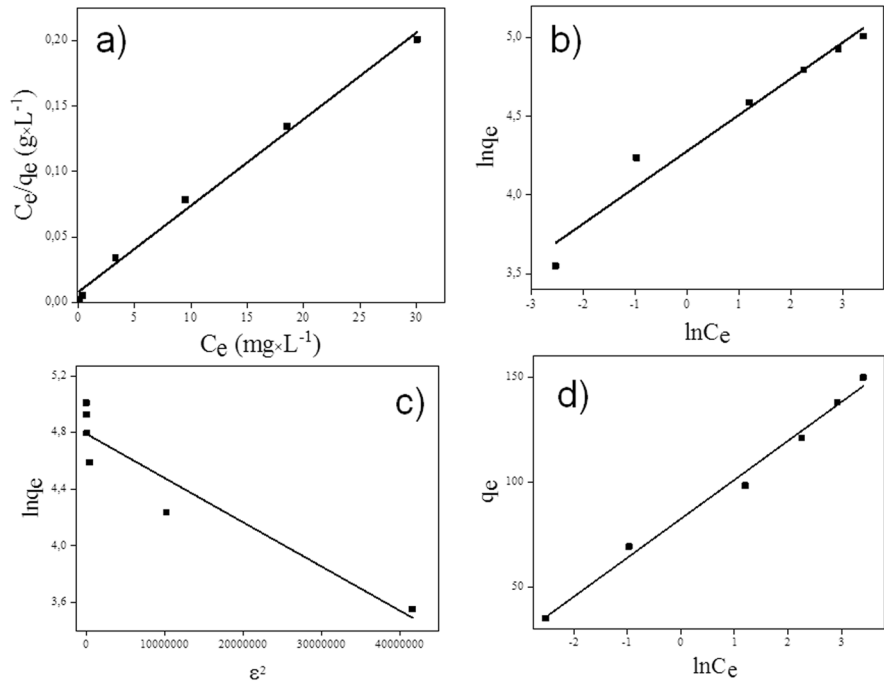


Table 5 Adsorption isotherm parameters of Langmuir, Freundlich, Dubinin Raduskevich, and Temkin isotherm models for MY and MB dyes on TmAC at 25 °C

MY	Langmuir				Freundlich		
	q_{max} (mg g ⁻¹)	K_L (L mg ⁻¹)	R^2	R_L	$1/n$	K_F (mg g ⁻¹) (L mg) ^{1/n}	R^2
	266.67	0.6856	0.9952	$0 < R_L < 1$	0.3079	104.97	0.8579
	Dubinin-Radushkevich (D-R)				Temkin		
	q_d (mg g ⁻¹)	β (mol ² kJ ⁻²)	E (kJ mol ⁻¹)	R^2	A_T (L g ⁻¹)	B_T (J mol ⁻¹)	R^2
	212.19	1.1272×10^{-7}	2.106	0.8892	15.114	56.932	0.9619
MB	Langmuir				Freundlich		
	q_{max} (mg g ⁻¹)	K_L (L mg ⁻¹)	R^2	R_L	$1/n$	K_F (mg g ⁻¹) (L mg ⁻¹) ^{1/n}	R^2
	151.52	0.8462	0.9924	$0 < R_L < 1$	0.2299	72.06	0.9511
	Dubinin-Radushkevich (D-R)				Temkin		
	q_d (mg g ⁻¹)	β (mol ² kJ ⁻²)	E (kJ mol ⁻¹)	R^2	A_T (L g ⁻¹)	B_T (J mol ⁻¹)	R^2
	120.36	3.1239×10^{-8}	4.002	0.8665	84.422	133.35	0.9877

4 Conclusion

Einkorn (*T. monococcum L.*) husks were used as a raw material to obtain TmAC. TmAC was characterized by different methods, such as elemental analysis, BET, SEM-EDX, FTIR-ATR, TGA-DTA, and pH_{ZPC} . The highest surface area was indicated

as 1321.01 m² g⁻¹ by using ZnCl₂ concentration of 2 (w/w) for TmAC. In this study, adsorbate concentration, contact time, initial MY and MB concentrations, temperature, and pH on TmAC were investigated in aqueous medium. Equilibrium data for both MY and MB were fitted well and were found to be $q_{max} = 266.67$ and $q_{max} = 151.52$ mg g⁻¹,

Table 6 Comparison of the maximum adsorption capacity (q_{max}) for MY and MB onto different activated carbons

Raw material	Activating agent	q_{max} (mg g ⁻¹)	Specific surface area (m ² g ⁻¹)	Reference
MY Gmelina arborea bark (PAAC)	H ₃ PO ₄	34.238	454.54	Isiuku and Nwabueze (2019)
Pitaya fruit peel (<i>Hylocereus undatus</i>) (HUPAC)	ZnCl ₂	144.07	667.30	Georgin et al. (2022)
Peanut shells (PnsAC)	H ₃ PO ₄	66.70	965.678	Garg et al. (2019)
Einkorn husks (<i>T. monococcum</i> L.) (TmAC)	ZnCl ₂	266.67	1321.01	This study
MB Apricot stones (ASAC)	H ₃ PO ₄ + HNO ₃	36.68	359.40	Djilani et al. (2015)
Watermelon (<i>Citrullus lanatus</i>) Rind (WAC)	ZnCl ₂	231.48	1156.00	Üner et al. (2016)
Sorghum residues (ACZ)	ZnCl ₂	386.10	1817.00	Khalil et al. (2017)
<i>Moringa oleifera</i> leaf (ACB)	NaOH	136.99	1.6881	Do et al. (2021)
Einkorn husks (<i>T. monococcum</i> L.) (TmAC)	ZnCl ₂	151.52	1321.01	This study

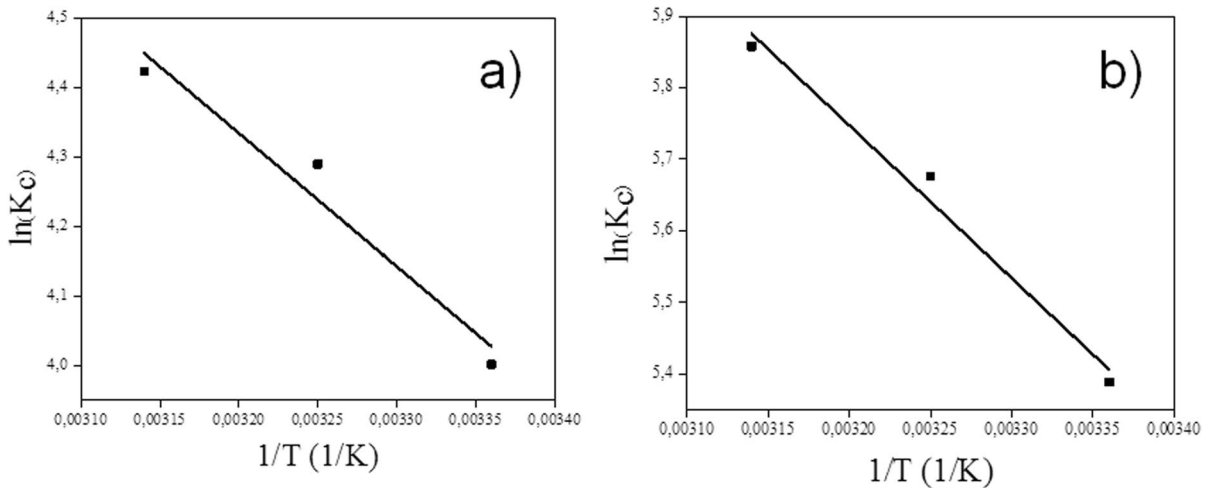


Fig. 13 Van't Hoff plot for **a** MY and **b** MB

respectively. The rate of adsorption is found to follow PSO kinetic model, and parameters calculated

Table 7 Thermodynamics for removal effects of MY and MB at various temperature

	Temperature (K)	ΔG° (kJ mol ⁻¹)	ΔH° (kJ mol ⁻¹)	ΔS° (kJ mol ⁻¹ K ⁻¹)
MY	298	-9.91	15.92	0.087
	308	-10.98		
	318	-11.69		
MB	298	-13.35	17.76	0.105
	308	-14.53		
	318	-15.49		

from this kinetic model are considerable closely experimental parameters.

The spontaneous and feasible adsorption of both MY and MB dyes on TmAC was demonstrated by negative ΔG° values obtained from thermodynamic study. The positive value of ΔH° was shown that the adsorption of MY and MB dyes was reversible and endothermic behavior. In addition, kinetic, thermodynamic, and equilibrium studies showed that both MY and MB adsorption on TmAC was used as an efficient and affordably convenient adsorbent. As a result, the activated carbon obtained from Einkorn (*T. monococcum* L.) husks is an efficient and cheap adsorbent for the removal of MY and MB from aqueous media.

Acknowledgements We would like to thank Trakya University, Scientific Research Project Unit (project no. 2018-180). We wish to thank Prof. Dr. Murat Turkyilmaz (Trakya Uni., Chemistry Dep., Inorganic Chem. Div.) for his TGA-DTA measurements.

Funding Open access funding provided by the Scientific and Technological Research Council of Türkiye (TÜBİTAK).

Data Availability Data will be available on reasonable request.

Declarations

Ethics Approval This paper is approved by all authors, and there is no conflict of interest for publication.

Conflict of Interest The authors declared no competing interests.

Open Access This article is licensed under a Creative Commons Attribution 4.0 International License, which permits use, sharing, adaptation, distribution and reproduction in any medium or format, as long as you give appropriate credit to the original author(s) and the source, provide a link to the Creative Commons licence, and indicate if changes were made. The images or other third party material in this article are included in the article's Creative Commons licence, unless indicated otherwise in a credit line to the material. If material is not included in the article's Creative Commons licence and your intended use is not permitted by statutory regulation or exceeds the permitted use, you will need to obtain permission directly from the copyright holder. To view a copy of this licence, visit <http://creativecommons.org/licenses/by/4.0/>.

References

- Abbas, M., & Trari, M. (2015). Kinetic, equilibrium and thermodynamic study on the removal of Congo Red from aqueous solutions by adsorption onto apricot stone. *Process Safety and Environmental Protection*, 98, 424–436. <https://doi.org/10.1016/j.psep.2015.09.015>
- Abdullah, S. S., Yusup, S., Ahmad, M. M., Ramli, A., & Ismail, L. (2010). Thermogravimetry study on pyrolysis of various lignocellulosic biomass for potential hydrogen production. *International Journal of Chemical and Molecular Engineering*, 4(12), 750–754.
- Aguayo-Villarreal, I. A., Hernández-Montoya, V., Bonilla-Petriciolet, A., Tovar-Gómez, R., Ramírez-López, E. M., & Montes-Morán, M. A. (2013). Role of acid blue 25 dye as active site for the adsorption of Cd²⁺ and Zn²⁺ using activated carbons. *Dyes and Pigments*, 96(2), 459–466. <https://doi.org/10.1016/j.dyepig.2012.08.027>
- Ahmad, A. A., Al-Raggad, M., & Shareef, N. (2021). Production of activated carbon derived from agricultural by-products via microwave-induced chemical activation: A review. *Carbon Letters*, 31, 957–971. <https://doi.org/10.1007/s42823-020-00208-z>
- Alberti, G., Amendola, V., Pesavento, M., & Biesuz, R. (2012). Beyond the synthesis of novel solid phases: Review on modelling of sorption phenomena. *Coordination Chemistry Reviews*, 256(1–2), 28–45. <https://doi.org/10.1016/j.ccr.2011.08.022>
- Aluigi, A., Rombaldoni, F., Tonetti, C., & Jannoke, L. (2014). Study of Methylene Blue adsorption on keratin nanofibrous membranes. *Journal of Hazardous Materials*, 268, 156–165. <https://doi.org/10.1016/j.jhazmat.2014.01.012>
- Auta, M., & Hameed, B. H. (2011). Optimized waste tea activated carbon for adsorption of Methylene Blue and Acid Blue 29 dyes using response surface methodology. *Chemical Engineering Journal*, 175, 233–243. <https://doi.org/10.1016/j.cej.2011.09.100>
- Avelar, F. F., Bianchi, M. L., Gonçalves, M., & da Mota, E. G. (2010). The use of piassava fibers (*Attalea funifera*) in the preparation of activated carbon. *Bioresource Technology*, 101(12), 4639–4645. <https://doi.org/10.1016/j.biortech.2010.01.103>
- Ayawei, N., Ebelegi, A. N., & Wankasi, D. (2017). Modeling and interpretation of adsorption isotherms. *Journal of Chemistry*, 2017, 1–11. <https://doi.org/10.1155/2017/3039817>
- Azam, K., Shezad, N., Shafiq, I., Akhter, P., Akhtar, F., Jamil, F., ... & Hussain, M. (2022). A review on activated carbon modifications for the treatment of wastewater containing anionic dyes. *Chemosphere*, 306, 135566. <https://doi.org/10.1016/j.chemosphere.2022.135566>
- Azani, M., Silmi, N. F., Chuin, C. T. H., Abdullah, N. S., Sharifuddin, S. S., & Hussin, M. H. (2019). Characterisation and Kinetic Studies on Activated Carbon Derived from Rubber Seed Shell for the Removal of Methylene Blue in Aqueous Solutions. *Journal of Physical Science*, 30(2), 1–20. <https://doi.org/10.21315/jps2019.30.2.1>
- Azari, A., Nabizadeh, R., Nasserli, S., Mahvi, A. H., & Mesdaghinia, A. R. (2020). Comprehensive systematic review and meta-analysis of dyes adsorption by carbon-based adsorbent materials: Classification and analysis of last decade studies. *Chemosphere*, 250, 126238. <https://doi.org/10.1016/j.chemosphere.2020.126238>
- Benhachem, F. Z., Attar, T., & Bouabdallah, F. (2019). Kinetic study of adsorption methylene blue dye from aqueous solutions using activated carbon. *Chemical Review and Letters*, 2(1), 33–39. <https://doi.org/10.1016/j.cej.2005.12.012>
- Benosmane, N., Boutemour, B., Hamdi, S. M., & Hamdi, M. (2022). Removal of methylene blue dye from aqueous solutions using polymer inclusion membrane technology. *Applied Water Science*, 12(5), 1–11. <https://doi.org/10.1007/s13201-022-01627-1>
- Brandolini, A., Hidalgo, A., & Moscaritolo, S. (2008). Chemical composition and pasting properties of einkorn (*Triticum monococcum* L. subsp. monococcum) whole meal flour. *Journal of Cereal Science*, 47(3), 599–609. <https://doi.org/10.1016/j.jcs.2007.07.005>
- Brandolini, A., Lucisano, M., Mariotti, M., & Hidalgo, A. (2018). A study on the quality of einkorn (*Triticum monococcum* L. ssp. monococcum) pasta. *Journal of Cereal Science*, 82, 57–64. <https://doi.org/10.1016/j.jcs.2018.05.010>

- Celebi, O., Üzümlü, Ç., Shahwan, T., & Erten, H. N. (2007). A radiotracer study of the adsorption behavior of aqueous Ba²⁺ ions on nanoparticles of zero-valent iron. *Journal of Hazardous Materials*, 148(3), 761–767. <https://doi.org/10.1016/j.jhazmat.2007.06.122>
- Chen, Y., Zhu, Y., Wang, Z., Li, Y., Wang, L., Ding, L., ... & Guo, Y. (2011). Application studies of activated carbon derived from rice husks produced by chemical-thermal process—A review. *Advances in colloid and interface science*, 163(1), 39–52. <https://doi.org/10.1016/j.cis.2011.01.006>
- Chowdhury, S., & Saha, P. (2010). Sea shell powder as a new adsorbent to remove Basic Green 4 (Malachite Green) from aqueous solutions: Equilibrium, kinetic and thermodynamic studies. *Chemical Engineering Journal*, 164(1), 168–177. <https://doi.org/10.1016/j.cej.2010.08.050>
- Dağdelen, S., Acemioğlu, B., Baran, E., & Koçer, O. (2014). Removal of remazol brilliant blue R from aqueous solution by pirina pretreated with nitric acid and commercial activated carbon. *Water, Air, & Soil Pollution*, 225, 1–15. <https://doi.org/10.1007/s11270-014-1899-8>
- Daoud, M., Benturki, O., Girods, P., Donnot, A., & Fontana, S. (2019). Adsorption ability of activated carbons from Phoenix dactylifera rachis and Ziziphus jujube stones for the removal of commercial dye and the treatment of dye-stuff wastewater. *Microchemical Journal*, 148, 493–502. <https://doi.org/10.1016/j.microc.2019.05.022>
- Dimov, I., Nakov, G., Ivanova, N., & Stamatovska, V. (2019). Effect of the process of flaking of einkorn (*Triticum monococcum* L.) on some basic chemical properties and biologically active compounds in the flaked product. *Journal of Central European Agriculture*, 20(4), 1210–1215. <https://doi.org/10.5513/JCEA01/20.4.2390>
- Djilani, C., Zaghoudi, R., Djazi, F., Bouhekima, B., Lallam, A., Modarressi, A., & Rogalski, M. (2015). Adsorption of dyes on activated carbon prepared from apricot stones and commercial activated carbon. *Journal of the Taiwan Institute of Chemical Engineers*, 53, 112–121. <https://doi.org/10.1016/j.jtice.2015.02.025>
- Do, T. H., Dung, N. Q., Chu, M. N., Van Kiet, D., Ngan, T. T. K., & Van Tan, L. (2021). Study on methylene blue adsorption of activated carbon made from Moringa oleifera leaf. *Materials Today: Proceedings*, 38, 3405–3413. <https://doi.org/10.1016/j.matpr.2020.10.834>
- Du, H., Cheng, J., Wang, M., Tian, M., Yang, X., & Wang, Q. (2020). Red dye extracted sappan wood waste derived activated carbons characterization and dye adsorption properties. *Diamond and Related Materials*, 102, 107646. <https://doi.org/10.1016/j.diamond.2019.107646>
- Dubinina, M. M., & Radushkevich, L. V. (1947). The equation of the characteristic curve of activated charcoal. *Proc Academy of Sciences of the USSR Physical Chemistry Section.*, 55, 331–337.
- Duman, O., Tunç, S., Polat, T. G., & Bozoğlan, B. K. (2016). Synthesis of magnetic oxidized multiwalled carbon nanotube-κ-carrageenan-Fe₃O₄ nanocomposite adsorbent and its application in cationic Methylene Blue dye adsorption. *Carbohydrate Polymers*, 147, 79–88. <https://doi.org/10.1016/j.carbpol.2016.03.099>
- Erdogan, T., & Oguz Erdogan, F. (2016). Characterization of the adsorption of disperse yellow 211 on activated carbon from cherry stones following microwave-assisted phosphoric acid treatment. *Analytical Letters*, 49(7), 917–928. <https://doi.org/10.1080/00032719.2015.1086776>
- Freundlich, H. M. F. (1906). Über die Adsorption in Lösungen. *Zeitschrift Für Physikalische Chemie*, 57, 387–470.
- Ganguly, P., Sarkhel, R., & Das, P. (2020). Synthesis of pyrolyzed biochar and its application for dye removal: Batch, kinetic and isotherm with linear and non-linear mathematical analysis. *Surfaces and Interfaces*, 20, 100616. <https://doi.org/10.1016/j.surfin.2020.100616>
- Gao, Y., Yue, Q., Gao, B., & Li, A. (2020). Insight into activated carbon from different kinds of chemical activating agents: A review. *Science of the Total Environment*, 746, 141094. <https://doi.org/10.1016/j.scitotenv.2020.141094>
- Garg, D., Kumar, S., Sharma, K., & Majumder, C. B. (2019). Application of waste peanut shells to form activated carbon and its utilization for the removal of acid yellow 36 from wastewater. *Groundwater for Sustainable Development*, 8, 512–519. <https://doi.org/10.1016/j.gsd.2019.01.010>
- Geçgel, Ü., Kocabıyık, B., & Üner, O. (2015). Adsorptive removal of methylene blue from aqueous solution by the activated carbon obtained from the fruit of catalpa bigonioides. *Water, Air, & Soil Pollution*, 226, 1–14. <https://doi.org/10.1007/s11270-015-2513-4>
- Geçgel, Ü., Üner, O., Gökara, G., & Bayrak, Y. (2016). Adsorption of cationic dyes on activated carbon obtained from waste Elaeagnus stone. *Adsorption Science & Technology*, 34(9–10), 512–525. <https://doi.org/10.1177/02636174166669727>
- Georgina, J., da Boit Martinello, K., Franco, D. S., Netto, M. S., Piccilli, D. G., Yilmaz, M., ... & Dotto, G. L. (2022). Residual peel of pitaya fruit (*Hylocereus undatus*) as a precursor to obtaining an efficient carbon-based adsorbent for the removal of metanil yellow dye from water. *Journal of Environmental Chemical Engineering*, 10(1), 107006. <https://doi.org/10.1016/j.jece.2021.107006>
- Gui, L., Peng, J., Li, P., Peng, R., Yu, P., & Luo, Y. (2019). Electrochemical degradation of dye on TiO₂ nanotube array constructed anode. *Chemosphere*, 235, 1189–1196. <https://doi.org/10.1016/j.chemosphere.2019.06.170>
- Hameed, B. H., Tan, I. A. W., & Ahmad, A. L. (2008). Adsorption isotherm, kinetic modeling and mechanism of 2, 4, 6-trichlorophenol on coconut husk-based activated carbon. *Chemical Engineering Journal*, 144(2), 235–244. <https://doi.org/10.1016/j.cej.2008.01.028>
- Hassan, W., Noureen, S., Mustaqeem, M., Saleh, T. A., & Zafar, S. (2020). Efficient adsorbent derived from Haloxylon recurvum plant for the adsorption of acid brown dye: Kinetics, isotherm and thermodynamic optimization. *Surfaces and Interfaces*, 20, 100510. <https://doi.org/10.1016/j.surfin.2020.100510>
- He, S., Chen, G., Xiao, H., Shi, G., Ruan, C., Ma, Y., ... & Yang, X. (2021). Facile preparation of N-doped activated carbon produced from rice husk for CO₂ capture. *Journal of Colloid and Interface Science*, 582, 90–101. <https://doi.org/10.1016/j.jcis.2020.08.021>
- Hendek Ertop, M. (2019). Comparison of industrial and home-made bulgur produced from einkorn wheat (*Triticum*

- monococcum*) and durum wheat (*Triticum durum*): Physicochemical, nutritional and microtextural properties. *Journal of Food Processing and Preservation*, 43(2), e13863. <https://doi.org/10.1111/jfpp.13863>
- Hesas, R. H., Arami-Niya, A., Daud, W. M. A. W., & Sahu, J. N. (2013). Preparation of granular activated carbon from oil palm shell by microwave-induced chemical activation: Optimisation using surface response methodology. *Chemical Engineering Research and Design*, 91(12), 2447–2456. <https://doi.org/10.1016/j.cherd.2013.06.004>
- Ihaddaden, S., Aberkane, D., Boukerroui, A., & Robert, D. (2022). Removal of methylene blue (basic dye) by coagulation-flocculation with biomaterials (bentonite and *Opuntia ficus indica*). *Journal of Water Process Engineering*, 49, 102952. <https://doi.org/10.1016/j.jwpe.2022.102952>
- Isiuku, B. O., & Nwabueze, B. I. (2019). Aqueous phase adsorption of metanil yellow on phosphoric acid-activated carbon prepared from GMELINA ARBOREA bark. *Journal of Chemical Society of Nigeria*, 44(1), 30–40.
- Kang, L., Li, J., Zeng, J., Gao, W., Xu, J., Cheng, Z., ... & Wang, B. (2019). A water solvent-assisted condensation polymerization strategy of superhydrophobic lignocellulosic fibers for efficient oil/water separation. *Journal of Materials Chemistry A*, 7(27), 16447–16457. <https://doi.org/10.1039/c9ta04815d>
- Keçeli, A. (2019). A review on the bioactive, antioxidant properties of einkorn (*triticum monococcum* L. ssp. *monococcum*) populations and using in organic agriculture. *Turkish Journal of Agriculture-Food Science and Technology*, 7(12), 2111–2120. <https://doi.org/10.24925/turjaf.v7i12.2111-2120.2833>
- Khalil, K. M., Allam, O. A., Khairy, M., Mohammed, K. M., Elkhatib, R. M., & Hamed, M. A. (2017). High surface area nanostructured activated carbons derived from sustainable sorghum stalk. *Journal of Molecular Liquids*, 247, 386–396. <https://doi.org/10.1016/j.molliq.2017.09.090>
- Kishor, R., Saratale, G. D., Saratale, R. G., Ferreira, L. F. R., Bilal, M., Iqbal, H. M., & Bharagava, R. N. (2021). Efficient degradation and detoxification of methylene blue dye by a newly isolated ligninolytic enzyme producing bacterium *Bacillus albus* MW407057. *Colloids and Surfaces b: Biointerfaces*, 206, 111947. <https://doi.org/10.1016/j.colsurfb.2021.111947>
- Kumar, A., & Jena, H. M. (2017). Adsorption of Cr (VI) from aqueous phase by high surface area activated carbon prepared by chemical activation with ZnCl₂. *Process Safety and Environmental Protection*, 109, 63–71. <https://doi.org/10.1016/j.psep.2017.03.032>
- Lagergren, S. K. (1898). About the theory of so-called adsorption of soluble substances. *Kungliga Svenska Vetenskapsakademiens Handlingar*, 24, 1–39.
- Langmuir, I. (1916). The constitution and fundamental properties of solids and liquids. Part I. Solids. *Journal of the American Chemical Society*, 38(11), 2221–2295.
- Lu, J., Batjikh, I., Hurh, J., Han, Y., Ali, H., Mathiyalagan, R., ... & Yang, D. C. (2019). Photocatalytic degradation of methylene blue using biosynthesized zinc oxide nanoparticles from bark extract of *Kalopanax septemlobus*. *Optik*, 182, 980–985. <https://doi.org/10.1016/j.ijleo.2018.12.016>
- Ma, J., Huang, D., Zou, J., Li, L., Kong, Y., & Komarneni, S. (2015). Adsorption of methylene blue and Orange II pollutants on activated carbon prepared from banana peel. *Journal of Porous Materials*, 22(2), 301–311. <https://doi.org/10.1007/s10934-014-9896-2>
- Milonjić, S. K., Ruvarac, A. L., & Šušić, M. V. (1975). The heat of immersion of natural magnetite in aqueous solutions. *Thermochimica Acta*, 11(3), 261–266. [https://doi.org/10.1016/0040-6031\(75\)85095-7](https://doi.org/10.1016/0040-6031(75)85095-7)
- Mortada, W. I., Mohamed, R. A., Abdel Morem, A. A., Awad, M. M., & Hassas, A. F. (2023). Effect and low-cost adsorption produce for removing chemical oxygen demand from wastewater using chemically activated carbon derived from rice husk. *Separations*, 10, 43–56. <https://doi.org/10.3390/separations10010043>
- Nakov, G., Brandolini, A., Ivanova, N., Dimov, I., & Stamatovska, V. (2018). The effect of einkorn (*Triticum monococcum* L.) whole meal flour addition on physico-chemical characteristics, biological active compounds and in vitro starch digestion of cookies. *Journal of Cereal Science*, 83, 116–122. <https://doi.org/10.1016/j.jcs.2018.08.004>
- Nirmaladevi, S., & Palanisamy, N. (2019). Preparation And Adsorptive Properties Of Activated Carbon From Acacia Leucophloea Wood Sawdust Hydrochar By Zinc Chloride Activation. *Cellulose Chemistry And Technology*, 53, 1029–1039. <https://doi.org/10.35812/CelluloseChemTech.2019.53.101>
- Nourmoradi, H., Moghadam, K. F., Jafari, A., & Kamarehie, B. (2018). Removal of acetaminophen and ibuprofen from aqueous solutions by activated carbon derived from *Quercus Brantii* (Oak) acorn as a low-cost biosorbent. *Journal of Environmental Chemical Engineering*, 6(6), 6807–6815. <https://doi.org/10.1016/j.jece.2018.10.047>
- Olasehinde, E. F., Abegunde, S. M., & Adebayo, M. A. (2020). Adsorption isotherms, kinetics and thermodynamic studies of methylene blue dye removal using *Raphia taedigera* seed activated carbon. *Caspian Journal of Environmental Sciences*, 18(4), 329–344. <https://doi.org/10.22124/cjes.2020.4279>
- Özacar, M., Şengil, İ.A., & Türkmenler, H. (2008). Equilibrium and kinetic data, and adsorption mechanism for adsorption of lead onto valonia tannin resin. *Chemical Engineering Journal*, 143(1–3), 32–42. <https://doi.org/10.1016/j.cej.2007.12.005>
- Pallarés, J., González-Cencerrado, A., & Arauzo, I. (2018). Production and characterization of activated carbon from barley straw by physical activation with carbon dioxide and steam. *Biomass and Bioenergy*, 115, 64–73. <https://doi.org/10.1016/j.biombioe.2018.04.015>
- Parab, H., Sudersanan, M., Shenoy, N., Pathare, T., & Vaze, B. (2009). Use of agro-industrial wastes for removal of basic dyes from aqueous solutions. *Clean–Soil, Air, Water*, 37(12), 963–969. <https://doi.org/10.1002/clen.200900158>
- Prakash, M. O., Raghavendra, G., Ojha, S., & Panchal, M. (2021). Characterization of porous activated carbon prepared from arhar stalks by single step chemical activation method. *Materials Today: Proceedings*, 39, 1476–1481. <https://doi.org/10.1016/j.matpr.2020.05.370>
- Rahman, M. A., Ahmed, T., Salehin, I. N., & Hossain, M. D. (2017). Color removal from textile wastewater using date

- seeds activated carbon. *Bangladesh Journal of Scientific and Industrial Research*, 52(1), 31–42. <https://doi.org/10.3329/bjsir.v52i1.32083>
- Reza, K. M., Kurny, A. S. W., & Gulshan, F. (2017). Parameters affecting the photocatalytic degradation of dyes using TiO₂: A review. *Applied Water Science*, 7(4), 1569–1578. <https://doi.org/10.1007/s13201-015-0367-y>
- Saleem, J., Shahid, U. B., Hijab, M., Mackey, H., & McKay, G. (2019). Production and applications of activated carbons as adsorbents from olive stones. *Biomass Conversion and Biorefinery*, 9, 775–802. <https://doi.org/10.1007/s13399-019-00473-7>
- Sing, K. S. W., Everett, D. H., Haul, R. A. W., Moscou, L., Pierotti, R. A., Rouquerol, J., & Siemieniowska, T. (1985). Reporting physisorption data for gas/solid systems with special reference to the determination of surface area and porosity. *Pure and Applied Chemistry*, 57(4), 603–619.
- Song, S., Fan, J., He, Z., Zhan, L., Liu, Z., Chen, J., & Xu, X. (2010). Electrochemical degradation of azo dye CI Reactive Red 195 by anodic oxidation on Ti/SnO₂-Sb/PbO₂ electrodes. *Electrochimica Acta*, 55(11), 3606–3613. <https://doi.org/10.1016/j.electacta.2010.01.101>
- Sosa, J. A., Laines, J. R., García, D. S., Hernández, R., Zappi, M., & de los Monteros, A. E. E. (2023). Activated Carbon: A Review of Residual Precursors, Synthesis Processes, Characterization Techniques, and Applications in the Improvement of Biogas. *Environmental Engineering Research*, 28(3). <https://doi.org/10.4491/eer.2022.100>
- Temkin, M., & Pyzhev, V. (1940). Kinetics of the synthesis of ammonia on promoted iron catalysts. *Acta Physicochimica*, 12(1), 217–222.
- Thommes, M., Kaneko, K., Neimark, A. V., Olivier, J. P., Rodriguez-Reinoso, F., Rouquerol, J., & Sing, K. S. (2015). Physisorption of gases, with special reference to the evaluation of surface area and pore size distribution (IUPAC Technical Report). *Pure and Applied Chemistry*, 87(9–10), 1051–1069. <https://doi.org/10.1515/pac-2014-1117>
- Üner, O., Geçgel, Ü., & Bayrak, Y. (2016). Adsorption of methylene blue by an efficient activated carbon prepared from Citrullus lanatus rind: Kinetic, isotherm, thermodynamic, and mechanism analysis. *Water, Air, & Soil Pollution*, 227, 1–15. <https://doi.org/10.1007/s11270-016-2949-1>
- Üner, O., Geçgel, Ü., & Bayrak, Y. (2019). Preparation and characterization of mesoporous activated carbons from waste watermelon rind by using the chemical activation method with zinc chloride. *Arabian Journal of Chemistry*, 12(8), 3621–3627. <https://doi.org/10.1016/j.arabj.2015.12.004>
- Unugul, T., & Nigiz, F. U. (2020). Preparation and characterization an active carbon adsorbent from waste mandarin peel and determination of adsorption behavior on removal of synthetic dye solutions. *Water, Air, & Soil Pollution*, 231, 1–14. <https://doi.org/10.1007/s11270-020-04903-5>
- Valix, M., Cheung, W. H., & McKay, G. (2004). Preparation of activated carbon using low temperature carbonisation and physical activation of high ash raw bagasse for acid dye adsorption. *Chemosphere*, 56(5), 493–501. <https://doi.org/10.1016/j.chemosphere.2004.04.004>
- Wang, X., Jiang, C., Hou, B., Wang, Y., Hao, C., & Wu, J. (2018). Carbon composite lignin-based adsorbents for the adsorption of dyes. *Chemosphere*, 206, 587–596. <https://doi.org/10.1016/j.chemosphere.2018.04.183>
- Weber, T. W., & Chakravorty, R. K. (1974). Pore and solid diffusion models for fixed-bed adsorbents. *AIChE Journal*, 20(2), 228–238.
- Wei, Q., Chen, Z., Cheng, Y., Wang, X., Yang, X., & Wang, Z. (2019). Preparation and electrochemical performance of orange peel based-activated carbons activated by different activators. *Colloids and Surfaces a: Physicochemical and Engineering Aspects*, 574, 221–227. <https://doi.org/10.1016/j.colsurfa.2019.04.065>
- Xia, M., Shao, X., Sun, Z., & Xu, Z. (2020). Conversion of cotton textile wastes into porous carbons by chemical activation with ZnCl₂, H₃PO₄, and FeCl₃. *Environmental Science and Pollution Research*, 27, 25186–25196. <https://doi.org/10.1007/s11356-020-08873-3>
- Yagmur, E., Gokce, Y., Tekin, S., Semerci, N. I., & Aktas, Z. (2020). Characteristics and comparison of activated carbons prepared from oleaster (*Elaeagnus angustifolia* L.) fruit using KOH and ZnCl₂. *Fuel*, 267, 117232. <https://doi.org/10.1016/j.fuel.2020.117232>
- Yahya, M. A., Al-Qodah, Z., & Ngah, C. Z. (2015). Agricultural bio-waste materials as potential sustainable precursors used for activated carbon production: A review. *Renewable and Sustainable Energy Reviews*, 46, 218–235. <https://doi.org/10.1016/j.rser.2015.02.051>
- Zaharieva, M., & Monneveux, P. (2014). Cultivated einkorn wheat (*Triticum monococcum* L. subsp. monococcum): The long life of a founder crop of agriculture. *Genetic Resources and Crop Evolution*, 61, 677–706. <https://doi.org/10.1007/s10722-014-0084-7>
- Zhang, B., Li, F., Wu, T., Sun, D., & Li, Y. (2015). Adsorption of p-nitrophenol from aqueous solutions using nanographite oxide. *Colloids and Surfaces a: Physicochemical and Engineering Aspects*, 464, 78–88. <https://doi.org/10.1016/j.colsurfa.2014.10.020>
- Zhang, L., Xi, G., Zhang, J., Yu, H., & Wang, X. (2017). Efficient catalytic system for the direct transformation of lignocellulosic biomass to furfural and 5-hydroxymethylfurfural. *Bioresource Technology*, 224, 656–661. <https://doi.org/10.1016/j.biortech.2016.11.097>

Publisher's Note Springer Nature remains neutral with regard to jurisdictional claims in published maps and institutional affiliations.